Emodin induced necroptosis in prostate cancer cells *via* the mitochondrial fission HSP90/MLKL/PGAM pathway

Xi Zhou
Central South University
Farjana Yeasmin Khusbu
Central South University
Yang Xie (xy11105@csu.edu.cn)
Xiangya Hospital of Central South University

Research Article

Keywords: Prostate cancer, Emodin, Necroptosis, PGAM, HSP90

Posted Date: July 26th, 2022

DOI: https://doi.org/10.21203/rs.3.rs-1895647/v1

Abstract

Background

Currently, prostate cancer is one of the major malignant tumors for males. Natural products from TCM are acknowledged as excellent anticancer agents to fight sensitive and resistant prostate cancer. We aimed to explore the potential mechanism and molecular targets of emodin (EG) against human prostate cancer cells based on RNA-sequencing measures and molecular biology techniques.

Methods

Seven robustaflavones and EG isolated from *Selaginella trichoclada were* identified by UV, HRESIMS, and 1D/2D NMR spectral techniques. Human prostate cancer PC3 and DU145 cells were evaluated to explore the potential mechanism and molecular targets of emodin by RNA-sequencing measure and KEGG functional enrichment analysis. We further verified the accuracy of the prediction results by colony formation assay, Hoechst 33258 stainings, TEM cell morphology analysis, qPCR, and western blot.

Results

RNA-sequencing measure and KEGG functional enrichment analysis revealed that the necroptosis-related pathway was activated upon EG treatment in PC3 cells. Furthermore, EG significantly decreased the cell viability of PC3 and DU145 cells and strikingly induced non-apoptotic cell death via necroptosis that was visualized through colony formation assay, Hoechst 33258 staining, and TEM analysis. mRNA and protein expression of necroptosis markers were analyzed by qPCR and immunoblotting, which implied that EG induced cell necroptosis via enhancing the expression of MLKL and HSP90AA1 activating PGAM pathway which is considered as a key mediator of mitochondrial fission and leading to ROS generation in PC3 and DU145 cells.

Conclusions

Our findings suggested that EG is a new small molecule agonist that induced necroptosis in prostate cancer cells via the mitochondrial fission HSP90/MLKL/PGAM pathway.

Background

Nowadays, cancer is the most dangerous disease worldwide, and tens of millions of patients are eventually diagnosed with it each year. Prostate cancer is a global disease, the incidence, and mortality of which rank it as the second most common cancer-causing death in men worldwide [1]. Chemotherapy is the optimum strategy to augment survival rates and is convenient for treating prostate cancer in the current situation. However, MDR of prostate cancer is one of the main obstacles to achieving successful

treatment and management of chemotherapy. It is noted that activation of the anti-apoptotic systems prompts cancer cells to escape this program leading to uncontrolled proliferation resulting in tumor survival, MDR, and recurrence of prostate cancer [2]. Thus, new chemotherapy agents or lead compounds are deserved to find, which induce new programmed cell death mechanisms against prostate cancer to overcome apoptosis resistance.

Necroptosis is an abnormal form of regulated necrotic cell death, which has been proved to be related to the defense mechanism in organisms against acute pancreatitis, retinal detachment, and cancer immunity [3, 4]. The main morphological features of necroptosis are rupture of the plasma membrane, cytoplasmic swelling, and moderate chromatin condensation, biochemical features of which include dropped ATP levels and activated RIP1, RIP3, and MLKL [5–8]. MLKL is a key mediator of necrosis signaling downstream of the kinase RIP3 and RIP5 [5]. The activation of PGAM5, a mitochondrial phosphatase, is another crucial component of necroptosis that can lead to the linear rupture of mitochondria, which is a very important segment in the early stage of cell necrosis. More interestingly, PGAM5 plays a pivotal role in the multiple pathways of necrotic cell death, such as excessive growth of oxygen free radicals and excessive leakage of calcium ions [6]. In addition, PGAM5 is the anchor of RIP1/RIP3/MLKL necrosome on mitochondria presenting a new pathway to induce necroptosis via the mitochondrial fission pathway that involves recruitment and activation of a GTPase DRP-1 [9–11]. Therefore, the investigators urged research to develop new chemotherapy agents that utilize necroptosis as a mechanism of action for fighting sensitive and resistant prostate cancer cell lines.

Many secondary metabolites of plants and their derivatives from TCM have been reported and served as attractive candidates for cancer prevention and treatment, which shows strong effects and low cytotoxicity for the patients [12]. Previous studies confirmed that natural compounds can be developed as excellent anticancer agents that induce necroptosis in prostate cancer [13–16].In the present study, *Selaginella trichoclada* was studied as a continuous program to explore strong and natural bioactive compounds from TCM of the family *Selaginella*, which has been used as folk medicines in China to treat jaundice, dysentery, burns, and cough with lung heat [17]. A systematic investigation of the chemical composition from the 70% EtOH extract of *Selaginella trichoclada* was undertaken. Eight compounds were isolated from *Selaginella trichoclada*, including seven biflavonoids and one anthraquinone. However, those isolated compounds have never been explored to assess their anticancer effects on prostate cancer and underlying molecular mechanism as well as whether they trigger necroptosis in prostate cancer cells.

Seven robustaflavones derivatives and one anthraquinone were identified based on extensive spectroscopic data including UV-vis, IR, HRESIMS, and 1D/2D NMR. The cytotoxicity of eight compounds was evaluated against human prostate cancer DU145 and PC3 cell lines by MTT methods. And we performed an RNA-sequencing measure on emodin (EG)-treated DU145 and PC3 cells to identify the mechanisms and the predictive biomarkers, which is a methodology for RNA profiling based on next-generation sequencing that enables to measure and compare gene expression patterns at an unprecedented resolution [18, 19]. Then, functional enrichment analysis based on the DEGs was performed, and the target genes were predicted to determine the regulatory relationship. Thus, we

attempted to explore the potential molecular regulatory mechanisms underlying the effect of EG in DU145 and PC3 cells.

Methods

Plant material

The whole herbs of *Selaginella trichoclada* were collected from Shimen (Hunan province, China) in August 2015, which was identified by Prof. Zhenji Li (Xiamen University, Xiamen, China). A voucher specimen (20150801) was deposited in the Xiangya School of Pharmaceutical Sciences, Central South University.

Extraction and isolation

The air-dried whole herbs of *S. trichoclada* (10.0 kg) were extracted with 70% EtOH (80 L × 2, 2h/each) under reflux conditions. The solvent was concentrated under reduced pressure to yield a dried residue (418.0 g), which was suspended in H_2O, then successively partitioned with petroleum ether, EtOAc, and *n*-BuOH. The EtOAc fractions (54.8 g) were preliminarily separated on silica gel CC with a gradient of CH_2Cl_2/MeOH (from 100:0 to 0:100, v/v) to obtain twelve fractions A-L (Fr. A-L). Then, Fr. C was subjected to Sephadex LH-20 with MeOH/H_2O (70/30, v/v, isocratic elution) to yield fifteen sub-fractions (Fr. C1-15). Fr. C5 was directly purified by Semi-preparative HPLC (ACN/H_2O, 45/55, v/v, 3.0 ml/min) to yield compounds **1** (5.1 mg), **3** (3.3 mg), and **4** (4.3 mg). Fr. C8 was then further purified by Semi-preparative HPLC (ACN/H_2O, 45/55, v/v, 3.0 ml/min) to afford compound **2** (4.5 mg), **5** (4.1 mg), **6** (3.8 mg), **7** (4.8 mg) and **8** (11.5 mg).

Cell cytotoxicity assay

Compounds **1-8** were evaluated to observe the effects on human prostate cancer DU145 and PC3 cell lines using the MTT assay (Multisciences, No. 70-MT000, Hangzhou, China). Briefly, DU145 and PC3 cells were seeded in 96-well cell culture plates (density: 1×10^5 cells/well) in RPMI-1640 (HAKATA) containing 10% FBS (MRC, Jiangsu, China) and 1% penicillin/streptomycin and incubated at 37 $^{\circ}$C and 5% CO_2. On the following day, the cells were treated with various concentrations of isolated compounds for 48 h. The cells were then treated with 10 μl of the MTT solution at 5 mg/mL for 4 hours followed by the addition of 150 μl of DMSO to each well. Finally, measurement of absorbance was carried out at 490 nm using an ELISA reader.

RNA extraction and sequencing

Total RNA was extracted using the mirVanaTM miRNA isolation Kit (Ambion) following the manufacturer's protocol. The quality and concentration of the total RNA were evaluated using Agilent 2100 Bioanalyzer (Agilent Technologies, Santa Clara, CA, USA). The samples with RNA Integrity Number (RIN) ≥ 7 were subjected to the subsequent analysis. The cDNA libraries were constructed using TruSeq Stranded mRNA LTSample Prep Kit (Illumina, San Diego, CA, USA) according to the manufacturer's instructions. Then these cDNA libraries were sequenced on the Illumina sequencing platform (Illumina HiSeqTM 2500) and 125bp/150bp paired-end reads were generated.

Bioinformatics analysis

Raw data (raw reads) were processed using Trimmomatic. The reads containing ploy-N and the low-quality reads were removed to obtain clean reads. Then the clean reads were mapped to the reference genome using hisat2. FPKM value of each gene was calculated using cufflinks, and the read counts of each gene were obtained by htseq-count [20-22].DEGs were identified using the DESeq R package functions estimate SizeFactors and nbinomTest. P-value < 0.05 and fold-change > 2 or < 0.5 were set as the threshold for significantly differential expression. Hierarchical cluster analysis of DEGs was performed to explore gene expression patterns [23].GO enrichment and KEGG pathway enrichment analysis of DEGs were respectively performed using R based on the hypergeometric distribution [24, 25].Then gene structure extension and novel transcripts identification were performed by comparing the reference genome and the known annotated genes using cuffcompare software.

Colony formation assay

DU145 and PC3 cells were seeded into 6-well plates (NEST Biotechnology Co. Ltd) and treated with different concentrations of EG after 24 h, then fresh medium containing 10% FBS was added to the wells. After incubating for 10-14 days, the colonies were fixed in methanol for 15 min and stained with 0.05% crystal violet. After being washed with PBS, the plates were photographed with a scanner (EPSON, JAPAN).

Morphological analysis by Hoechst 33258 staining assay

To investigate the cell apoptosis, morphological analysis was performed by Hoechst 33258 staining. Cells were fixed with methanol acetic acid for 10 min followed by staining with 100μl of Hoechst 33258 at room temperature in dark for 10 min. The cells were then washed twice with PBS, examined, and immediately photographed under a fluorescence microscope with an excitation wavelength of 330-380nm. Apoptotic cells were defined based on nuclear morphology changes, such as chromatin condensation and fragmentation.

Cell morphological assessment

DU145 and PC3 cells were seeded in a 6-well plate and treated with EG for 48 h. After a drug intervention, the images were observed using an inverted microscope (Leica, Germany). Meanwhile, cells were also grown in a 6 cm culture dish and treated with various concentrations of EG for 48 h. After, cells were harvested by trypsinization and combined with supernatant, followed by centrifugation at 2500 rpm at 4 °C for 5 min and fixing in 2.5% glutaraldehyde for 2 h. The cell precipitate was washed with PBS three times, post-fixed in 1% osmium tetroxide buffer, dehydrated in a graded series of ethanol, and embedded in spur resin. The thin sections (50 to 60 nm) were cut with an ultramicrotome and stained with saturated solutions of uranyl acetate combined with lead citrate and later observed using TEM HT7700 (HITACHI, Japan).

Reactive oxygen species (ROS) measurement

The production of ROS in DU145 and PC3 cells was measured after EG treatment using a cellular ROS assay kit (UE, No. R6033-1000T, Suzhou, China). The DCFH-DA is easily oxidized to fluorescent DCF for the detection of intracellular ROS in DU145 and PC3 cells treated with EG and DMSO (solvent control) as previously described, respectively. DCF was imaged by fluorescence microscopy (Carl Zeiss, Germany).

RT-PCR analysis

Prostate cancer cell lines PC3 and DU145 were cultured in RPMI-1640 containing 10% heat-inactivated FBS and 1% penicillin/streptomycin. All cells were incubated in an incubator with 5% CO_2 at 37 °C. Real-time PCR was conducted to evaluate gene expression. Total RNA was extracted from cells using an RNA Isolator (New Cell & Molecular Biotech, No. M050, Suzhou, China). cDNA was synthesized from total RNA by reverse transcription kit (Vazyme Biotech Co., Ltd, No. R302, Nanjing, China). The RT-PCR reactions were performed by ChamQ SYBR qPCR Master Mix. The reaction primers are as follows:

PGAM5-fwd: ATCTGTCACGCCAACGTCATCC

PGAM5-rve: CAGCAAGTGAAAGAGGTCAGGAC

HSP90AA1-fwd: GCCGCCCCTGGAAGGAGACGACGACACG

HSP90AA1-rve: GCCAGGCGAGCCTCGGCAGCGCTCA

GAPDH-fwd: GTCTCCTCTGACTTCAACAGCG

GAPDH-rve: ACCACCCTGTTGCTGTAGCCAA

Immunofluorescence staining

DU145 and PC3 cells were seeded into 24 wells plate and treated at different concentrations of EG after 24 h. The cells were washed by PBS after 48 h, then fixed by 4% Paraformaldehyde for 30 min, and permeabilized with 0.1% Triton X-100 in PBS for 30 min. Cells were washed with PBS, blocked with 5% BSA in PBS for 2 h, and incubated with PGAM5 polyclonal antibody (Proteintech Group, Inc, 28445-1-AP, Wuhan, China) in 5% BSA at 4 ˚C overnight. After cells were washed with PBS, Cy3-conjugated secondary antibody (Proteintech Group, Inc, SA00009-2, Wuhan, China) was applied for 2 h in dark, and then PBS-washed cells were subjected to staining with DAPI for 3 min. Finally, cells were imaged by a fluorescence microscope (Zeiss, Germany).

Western blot analysis

The harvested cells were washed with PBS and lysed with protein lysis buffer (Beyotime Biotechnology, Shanghai, China). Protein concentrations of the proteins were determined by using a BCA Protein Assay Kit (FineTest, Wuhan, China). Sample proteins were separated by electrophoresis in sodium dodecyl sulfonate (SDS)-polyacrylamide gels, transferred onto a PVDF membrane (Merck Millipore, Billerica, MA) and incubated with the indicated PGAM5 polyclonal antibody (Proteintech Group, Inc, 28445-1-AP, Wuhan, China), HSP90 antibody (Cell Signaling Technology Inc, 48745, Boston, USA) and α-Tubulin antibody (Cell Signaling Technology Inc, 2144S, Boston, USA) at 4 ˚C overnight. After washing three times with TBST and incubating with the secondary antibody at room temperature for 2 h, the protein expression was detected by using an ECL Prime Western blotting Kit (NCM Biotech, P10100, Suzhou, China).

Statistical analysis

Statistical analysis was conducted by SPSS 18.0. Statistics data were shown as mean ± standard deviation. For difference comparison, Student’s t-test was conducted for two groups, respectively. P values less than 0.05 were considered statistically significant.

Results

Chemical structural elucidation

A systematic investigation of the chemical composition of the family *Selaginella* was undertaken. Eight compounds were isolated from the 70% EtOH extract of *Selaginella trichoclada*. Compounds **1**-**7** were the robustaflavone type derivates and identified as robustaflavone 7,5"-dimethyl ether (**1**), robustaflavone 7,4'-dimethyl ether (**2**), 2",3"-dihydrorobustaflavone 4',7"-dimethyl ether (**3**), 2,3,2",3"-tetrahydrorobustaflavone (**4**), 2,3,2",3"-tetrahydrorobustaflavone 7-methyl ether (**5**), 2,3,2",3"-tetrahydrorobustaflavone 4'-methyl ether (**6**), 2,3,2",3"-tetrahydrorobustaflavone 4'"-methyl ether (**7**), by comparing NMR data with literatures [17, 26-28],respectively. Compound **8** was identified as anthraquinones, emodin. The chemical structure of compounds **1-8** were shown in Fig. 1.

Emodin induced prostate cancer DU145 and PC3 cells death

To evaluate the effects of different concentrations of compounds **1-8** against prostate cancer cell proliferation, we used the MTT assay for testing cytotoxicity in DU145 and PC3 cells. 5-Fu and DMSO were treated as a positive and negative control, respectively. The results regarding the cytotoxic effects of all isolated compounds in human prostate cancer DU145 and PC3 cells were shown in Table 1. Results showed that the viability of DU145 and PC3 cells in the EG-treated-48 h group was significantly decreased than the negative control group with an IC_{50} value of 18.22 ± 0.76 μM, and 68.74 ± 5.93 μM, respectively (Fig. 2). Notably, EG did not clearly suppress liver cell proliferation (143.25 ± 18.9 μM), which suggested that the natural compound EG is less toxic to normal liver cells.

Emodin-induced PCa cell death was apoptosis-independent

Whether EG induces necroptosis in prostate cancer cells, the morphological changes of EG-treated DU145 and PC3 cells were observed using colony formation assay, Hoechest 33258 staining, and transmission electron microscopy (TEM) analysis. Cell morphology of DU145 and PC3 cells were clearly visible and the number of cells was significantly decreased as shown in Fig. 3A. Then, the long-term inhibitory effects of EG on DU145 and PC3 cell proliferation were studied through colony formation assay. The colony formation results showed that EG inhibited the proliferation and population dependence of DU145 and PC3 cells in a dose-dependent manner (Fig. 3B). In addition, staining with DNA-binding fluorochrome Hoechest 33258 showed the non-typical apoptotic nuclei condensation and fragmentation of chromatin in both of the cell lines (Fig. 3C). Besides, according to TEM analysis, the cell morphology of DU145 and PC3 after EG treatment exhibited none of the apoptosis-related cell morphological characteristics such as membrane blebbing and chromatin condensation. There was critical evidence that the rupture of the cellular membrane, progressively translucent cytoplasm, and swelling of organelles were visualized which are some of the classical features of necroptosis (Fig. 4). Thus, we concluded that there is a possibility of necroptosis execution induced by EG in DU145 and PC3 cells.

There is a close correlation between necroptosis and ROS's cellular content in determining cancer cells' fate. So, we urged to investigate the production of intracellular ROS in DU145 and PC3 and employed fluorescent dichlorofluorescein. The various concentrations of EG significantly induced intracellular ROS generation (green fluorescent) in DU145 and PC3 cells (Fig. 5). Thus, we inferred that EG induces prostate cancer cell death via necroptosis related to ROS accumulation.

Emodin-mediated PCa cell death via necroptosis

Afterward, we performed RNA-sequencing-based transcriptome analysis data on prostate cancer cells after being treated with EG. This high-throughput method allowed us to uncover the genes and pathways that were changed after EG treatment. Volcano plots of DEGs were shown in Fig .6A, the green and red colors representing down-expression and up-expression, respectively. A total of downregulated and upregulated genes (using 2-fold as the cut-off value) were identified based on RNA-sequencing data (Fig. 6B). KEGG analyses were applied to explore the biological functions of EG in prostate cancer, which suggested that highly enriched DEGs resulted after EG treatment in PC3 cells were associated with the necroptosis cell death pathway when compared with untreated cells (Fig. 6D). KEGG enrichment analysis results showed that DEGs such as CAMK2A, CAMK2B, H2AFY2, STAT6, PYGM, XIAP, TLR4, PARR4, IFNAR2, CASP8, and RIRK1 genes were all significantly downregulated by EG induction (Fig. 6C). Besides, BIRC3, PLA2G4A, TNFRSF10A, IL-1β, TICAM1, SQSTM1, HSP90AB1, PARP2, HIST1H2AE, MLKL, PPID, TNFAIP3, HSP90AA1, H2AFZ, PPIA, CHMP4A, FAF1, HIST2H2AC, RBCK1, SLC25A4, PGAM5, FTL, SLC25A5, VDAC2 and FTH1 genes were significantly upregulated following treatment with EG (Fig. 6C). Noted that MLKL and PGAM5 play a pivotal role in inducing necroptosis via the mitochondrial fission pathway [29].A previous large-scale study documented that the molecular chaperone heat shock protein 90 (HSP90AA1) is highly expressed in tumor tissues in most cancer types except prostate cancer, which is a potential diagnostic and prognostic factor for cancer [30].There is a great strategy that increase in the expressions of HSP90AA1 and PGAM5 inhibits cell proliferation in prostate cancer. Our findings provide a sight that EG could be a small molecule agonist to upregulate necroptosis in PC3 prostate cancer cells via the mitochondrial fission pathway.

Referred to those results of cell morphology analysis and RNA-sequence measure, we evaluated the expression of HSP90 and PGAM5 genes in DU145 and PC3 cells using RT-qPCR analysis. Fig. 7A is showing the heatmap of DE-mRNAs between the EG group and the control group, blue represents the upregulated PGAM5 and HSP90AA1 mRNA levels. Then, for further exploration of the cellular signaling mechanism of the EG effect against DU145 and PC3 cells, we analyzed the level of PGAM5 and HSP90AA1 genes. EG significantly up-regulated PGAM5 and HSP90AA1 gene expression, stipulating further evidence that EG could be considered a strong agonist featuring necroptosis as a cell-killing mechanism against prostate cancer cells (Fig. 7B and 7C). Interestingly, PGAM5 and HSP90AA1 mRNA expression was increased in a dose-dependent manner in PC3 cells (Fig. 7B). These results indicate that

the mitochondrial fission HSP90/MLKL/PGAM signaling is critical for EG-induced necroptosis in PC3 cells.

To further confirm the results, we investigated the expression of PGAM5 protein by immunofluorescence staining. As shown in Fig.8, fluorescence imaging exhibited that EG treatment induced the expression of PGAM5 protein in DU145 and PC3 cells in a dose-dependent manner (the red colors represent PGAM5 protein). Interestingly enough, PGAM5 protein appeared in the nucleus of DU145 and PC3 cells after EG treatment. PGAM5 is responsible for the execution of the early stage of necroptosis, which consists of the activation of mitochondrial fission, Ca^{2+} overload, and excessive ROS generation leading to mitochondrial fragmentation and disruption of mitochondrial movement which eventually evoke cell death. Subsequently, further exploring the cellular signaling mechanism of the EG effect, we analyzed the protein level of HSP90 and PGAM5 using Western blotting. As shown in Fig. 9, compared with the control group, EG significantly increased the expression of HSP90 and PGAM5 proteins in DU145 and PC3 cells (Fig. 9). Finally, those findings provide strong evidence that EG induces necroptosis in prostate cancer via the mitochondrial fission HSP90/MLKL/PGAM pathway.

Discussion

For nearly four decades, natural products from herb medicines or plants remain a major source of lead compounds and candidate drug discovery, which have been confirmed to reduce infection rates and the mortality rate of different animal models [12]. Emodin is a naturally occurring anthraquinone derivative and an active ingredient of traditional Chinese herbs, which inhibits cell growth in several types of cancer cells and regulates genes and proteins related to the control of cell apoptosis, cell invasion, metastasis, and cell cycle arrest [8, 31]. Moreover, the synergistic enhancement of apoptosis is important in combination with chemotherapeutic agents for cancer and has attracted attention as a promising avenue of treatment [32]. However, many cancer cells are chemo-resistant or defective in apoptosis induction. Therefore, developing new agents that enhance different forms of non-apoptotic cell death will hopefully provide a promising therapeutic strategy for cancer patients.

In the present paper, we noted that Emodin-induced death in DU145 and PC3 prostate cancer cells are independent of apoptosis. There is a close correlation between necroptosis and ROS's cellular content in determining cancer cells' fate [11]. Moreover, we observed the accumulation of intracellular ROS generation, as well as the rupture of the cellular membrane, progressively translucent cytoplasm, and swelling of organelles in DU145 and PC3 cells which are typical features of the necroptosis process. Necroptosis is an abnormal form of necrotic cell death and plays a crucial role in cancer treatment, which is related to the defense mechanism in organisms against acute pancreatitis, retinal detachment, and cancer immunity [33]. Afterward, we performed RNA-sequencing-based transcriptome analysis data on prostate cancer cells after being treated with EG. Transcriptome analysis showed that BIRC3, PLA2G4A, TNFRSF10A, IL-1β, TICAM1, SQSTM1, HSP90AB1, PARP2, HIST1H2AE, MLKL, PPID, TNFAIP3, HSP90AA1, H2AFZ, PPIA, CHMP4A, FAF1, HIST2H2AC, RBCK1, SLC25A4, PGAM5, FTL, SLC25A5, VDAC2, and FTH1 genes were upregulated which are the regulatory genes of necroptosis cell death and could be considered

as potential targets of EG in prostate cancer treatment. and Inhibition of HSP90 blocks membrane translocation of activated MLKL, which implicates HSP90 as a modulator of necroptosis at the level of MLKL [34]. In human tumor cells, knockout of PGAM5 alleviates necroptosis induced by TNF-α, a calcium ionophore, and ROS, which plays a key role in oxidative stress-induced necroptosis [6]. PGAM5 increases the level of Cyclophilin D phosphorylation to open mitochondrial permeability transition pores (mPTPs) and increase ROS production, evoking endothelial necroptosis [11]. The opening of mPTPs is triggered mainly by the increase of the matrix Ca^{2+} concentration and oxidative stress [35, 36]. Above mentioned studies also confirm our findings that EG enhances the expression of the HSP90AA1 gene and activates the PGAM pathway leading to intracellular ROS generation. We determined that mitochondrial fission mediated by PGAM takes place in response to EG which ultimately results in necroptosis. The sketch map of the underlying molecular mechanisms associated with the anticancer effect of EG in PC3 and DU145 cells is illustrated in Fig. 10.

Conclusion

In summary, we presented a natural anthraquinone derivate EG that could potentially be a small molecule agonist in prostate cancer treatment inducing necroptosis via the mitochondrial fission HSP90/MLKL/PGAM pathway.

Declarations

Acknowledgments

Not applicable.

Author's Contributions

X. Zhou performed the experiments and analyzed the data. F.Y. Khusbu revised the manuscript. Y. Xie designed the experiments, analyzed the data, and wrote the manuscript. All authors read and approved the final manuscript.

Funding

This research was supported by the Hunan Provincial Natural Science Foundation of China (2022JJ40833).

Ethics statement

The experiments were conducted with the understanding and consent of each participant.

Consent for publication

Not applicable.

Conflict of interest

The authors declare that they have no known competing financial interests or personal relationships that could have appeared to influence the work reported in this paper.

Author Details

[a]Department of Orthopedics, Xiangya Hospital, Central South University, Changsha, PR China; [b]School of Life Sciences, Central South University, Changsha, PR China; [c]Xiangya School of Pharmaceutical Sciences, Central South University, Changsha, PR China; [d]National Clinical Research Center for Geriatric Disorders, Xiangya Hospital, Central South University, Changsha, PR China.

References

1. R.L. Siegel, K.D. Miller, A Jemal, Cancer statistics, 2020, CA Cancer J. Clin. 70(1) (2020) 7–30.
2. R.W. Johnstone, A.A. Ruefli, S.W. Lowe, Apoptosis: a link between cancer genetics and chemotherapy, Cell 108 (2) (2002) 153–164.
3. S. Fulda, The mechanism of necroptosis in normal and cancer cells, Cancer Biol. Ther. 14 (11) (2013) 999–1004.
4. Y. Gong, Z. Fan, G. Luo, C. Yang, Q. Huang, K. Fan, H. Cheng, K. Jin, Q. Ni, X. Yu, C. Liu, The role of necroptosis in cancer biology and therapy, Mol. Cancer 18 (1) (2019) 100.
5. X. Chen, W. Li, J. Ren, D. Huang, W.T. He, Y. Song, C. Yang, W. Li, X. Zheng, P. Chen, J. Han, Translocation of mixed lineage kinase domain-like protein to plasma membrane leads to necrotic cell death, Cell Res. 24 (1) (2014) 105–121.
6. Z. Wang, H. Jiang, S. Chen, F. Du, X. Wang, The mitochondrial phosphatase PGAM5 functions at the convergence point of multiple necrotic death pathways, Cell 148(1–2) (2012) 228–243.
7. K.J. Wang, K.Y. Wang, H.Z. Zhang, X.Y. Meng, J.F. Chen, P. Wang, J.H. Jiang, Q. Ma, Up-Regulation of RIP3 Alleviates Prostate Cancer Progression by Activation of RIP3/MLKL Signaling Pathway and Induction of Necroptosis, Front. Oncol. 10 (2020) 1720.
8. J. Zhou, G. Li, G. Han, S. Feng, Y. Liu, J. Chen, C. Liu, L. Zhao, F. Jin, Emodin induced necroptosis in the glioma cell line U251 via the TNF-α/RIP1/RIP3 pathway, Invest. New Drugs 38(1) (2020) 50–59.

9. L. She, H. Tu, Y.Z. Zhang, L.J. Tang, N.S. Li, Q.L. Ma, B. Liu, Q. Li, X.J. Luo, J. Peng, Inhibition of Phosphoglycerate Mutase 5 Reduces Necroptosis in Rat Hearts Following Ischemia/Reperfusion Through Suppression of Dynamin-Related Protein 1, Cardiovasc Drugs Ther. 33(1) (2019) 13–23.
10. C. Xue, X. Gu, G. Li, Z. Bao, L. Li, Mitochondrial Mechanisms of Necroptosis in Liver Diseases, Int. J. Mol. Sci. 22(1) (2020) 66.
11. S.L. Zhang, H.B. Tang, J.T. Hu, Z.L. Zang, X. Ding, S. Li, H. Yang, PGAM5-CypD pathway is involved in bromocriptine-induced RIP3/MLKL-dependent necroptosis of prolactinoma cells, Biomed. Pharmacother. 111 (2019) 638–648.
12. D.J. Newman, G.M. Cragg, Natural Products as Sources of New Drugs over the Nearly Four decades from 01/1981 to 09/2019, J. Nat. Prod. 83(3) (2020) 770–803.
13. A. Datta, H. Kim, M. Lal, L. McGee, A. Johnson, A.A. Moustafa, J.C. Jones, D. Mondal, M. Ferrer, A.B. Abdel-Mageed, Manumycin A suppresses exosome biogenesis and secretion via targeted inhibition of Ras/Raf/ERK1/2 signaling and hnRNP H1 in castration-resistant prostate cancer cells, Cancer Lett. 408 (2017) 73–81.
14. T. Costea, O.C. Vlad, L.C. Miclea, C. Ganea, J. Szollosiz, M.M. Mocanu, Alleviation of Multidrug Resistance by Flavonoid and Non-Flavonoid Compounds in Breast, Lung, Colorectal and Prostate Cancer, Int. J. Mol. Sci. 21 (2) (2020) 401.
15. F. Fontana, M. Raimondi, M. Marzagalli, A.D. Domizio, P. Limonta, Natural Compounds in Prostate Cancer Prevention and Treatment: Mechanisms of Action and Molecular Targets, Cells 9 (2) (2020) 460.
16. X. Wang, G. Fang, Y. Pang, Chinese Medicines in the Treatment of Prostate Cancer: From Formulas to Extracts and Compounds, Nutrients 10 (3) (2018) 283.
17. Y. Xie, X. Zhou, J. Li, X.C. Yao, W.L. Liu, F.H. Kang, Z.X. Zou, K.P. Xu, P.S. Xu, G.S. Tan, Identification of a new natural biflavonoids against breast cancer cells induced ferroptosis via the mitochondrial pathway. Bioorg. Chem. 109 (2021) 104744.
18. F. Finotello, B.D. Camillo, Measuring differential gene expression with RNA-seq: challenges and strategies for data analysis, Brief Funct. Genomics 14 (2) (2015) 130–142.
19. B. Hwang, J.H. Lee, D. Bang, Single-cell RNA sequencing technologies and bioinformatics pipelines, Exp. Mol. Med. 50 (8) (2018) 1–14.
20. S. Anders, P.T. Pyl, W. Huber, HTSeq-a Python framework to work with high-throughput sequencing data, Bioinformatics 31 (2) (2015) 166–169.
21. A. Roberts, C. Trapnell, J. Donaghey, J.L. Rinn, L. Pachter, Improving RNA-Seq expression estimates by correcting for fragment bias, Genome Biol. 12 (3) (2011) R22.
22. C. Trapnell, B.A. William, G. Pertea, A. Mortazavi, G. Kwan, J.V.B. Marijke, L.S. Steven, J.W. Barbara, P. Lior, Transcript assembly and quantification by RNA-Seq reveals unannotated transcripts and isoform switching during cell differentiation, Nat. Biotechnol. 28 (5) (2010) 511–515.
23. M. Kanehisa, M. Araki, S. Goto, M. Hattori, M. Hirakawa, M. Itoh, T. Katayama, S. Kawashima, S. Okuda, T. Tokimatsu, Y. Yamanishi, KEGG for linking genomes to life and the environment, Nucleic

Acids Res. 36 (2008) 480–484.
24. B. Langmead, S.L. Salzberg, Fast gapped-read alignment with Bowtie 2, Nat. Methods, 9 (4) (2012) 357–359.
25. A. Roberts, L. Pachter, Streaming fragment assignment for real-time analysis of sequencing experiments, Nat. Methods 10 (1) (2013) 71–73.
26. L.F. Liu, H.H. Sun, J.B. Tan, Q. Huang, F. Cheng, K.P. Xu, Z.X. Zou, G.S. Tan, New cytotoxic biflavones from *Selaginella doederleinii*, Nat Prod Res. 35(6) (2021) 930–936.
27. H. Zou, M.L. Yi, K.P. Xu, X.F. Sheng, G.S. Tan, Two new flavonoids from *Selaginella uncinate*, J Asian Nat Prod Res. 18(3) (2016) 248–252.
28. Z.X. Zou, S. Zhang, Tan, D.K. Chen, G.S. Tan, Two new biflavonoids from *Selaginella doederleinii*, Phytochem Lett. 40 (2020) 126–129.
29. Lu, J. Sun, J.S. Yoon, Y. Zhang, L. Zheng, E. Murphy, M.P. Mattson, M.J. Lenardo, Mitochondrial Protein PGAM5 Regulates Mitophagic Protection against Cell Necroptosis, PLoS One 11 (1) (2016) e0147792.
30. W. Chen, G. Li, J. Peng, W. Dai, Q. Su, Y. He, Transcriptomic analysis reveals that heat shock protein 90α is a potential diagnostic and prognostic biomarker for cancer, Eur. J. Cell Biol. 29 (4) (2020) 357–364.
31. X. Dong, J. Fu, X. Yin, S. Cao, X. Li, L. Lin, N.J. Huyiligeqi, Emodin: A Review of its Pharmacology, Toxicity and Pharmacokinetics, Phytother. Res. 30 (8) (2016) 1207–1218.
32. L. Huang, X.B. Wang, Q.M. Yu, Z.Z. Zhang, Synergistic cancer growth-inhibitory effect of emodin and low-dose cisplatin on gastric cancer cells in vitro, Trop J. Pharm. Res. 14 (8) (2015) 1427–1434.
33. J. Sprooten, D.P. Wijngaert, I. Vanmeerbeerk, S. Martin, P. Vangheluwe, S. Schlenner, D.V. Krysko, J.B. Parys, G. Bultynck, P. Vandenabeele, A.D. Garg, Necroptosis in Immuno-Oncology and Cancer Immunotherapy, Cells 9 (8) (2020) 1823.
34. S.L. Zhang, H.B. Tang, J.T. Hu, Z.L. Zang, X. Ding, S. Li, H. Yang, PGAM5-CypD pathway is involved in bromocriptine-induced RIP3/MLKL-dependent necroptosis of prolactinoma cells, Biomed. Pharmacother. 111 (2019) 638–648.
35. A.V. Jacobsen, K.N. Lowes, M.C. Tanzer, I.S. Lucet, J.M. Hildebrand, E.J. Petrie, V.M.F. Delft, Z. Liu, S.A. Conos, J.G. Zhang, D.C. Huang, J. Silke, G. Lessene, J.M. Murphy, HSP90 activity is required for MLKL oligomerisation and membrane translocation and the induction of necroptotic cell death, Cell Death Dis. 7 (1) (2016) e2051.
36. A.P. Halestrap, A.P. Richardson, The mitochondrial permeability transition: a current perspective on its identity and role in Ischaemia/Reperfusion injury, J. Mol. Cell Cardiol. 78 (2015) 129–141.

Tables

Cytotoxicity IC_{50} (μM)									
Compouds	**1**	**2**	**3**	**4**	**5**	**6**	**7**	**8**	**5-Fu**
PC3	19.04 ± 3.01	>100	42.42 ± 3.64	>100	20.21 ± 4.45	35.39 ± 2.45	30.93 ± 2.98	18.22 ± 0.76	67.91 ± 9.33
DU145	>100	>100	>100	>100	>100	62.47 ± 5.93	>100	68.74 ± 13.6	>100

Table 1 Cytotoxicity of compounds 1-8 against cancer cell lines

Figures

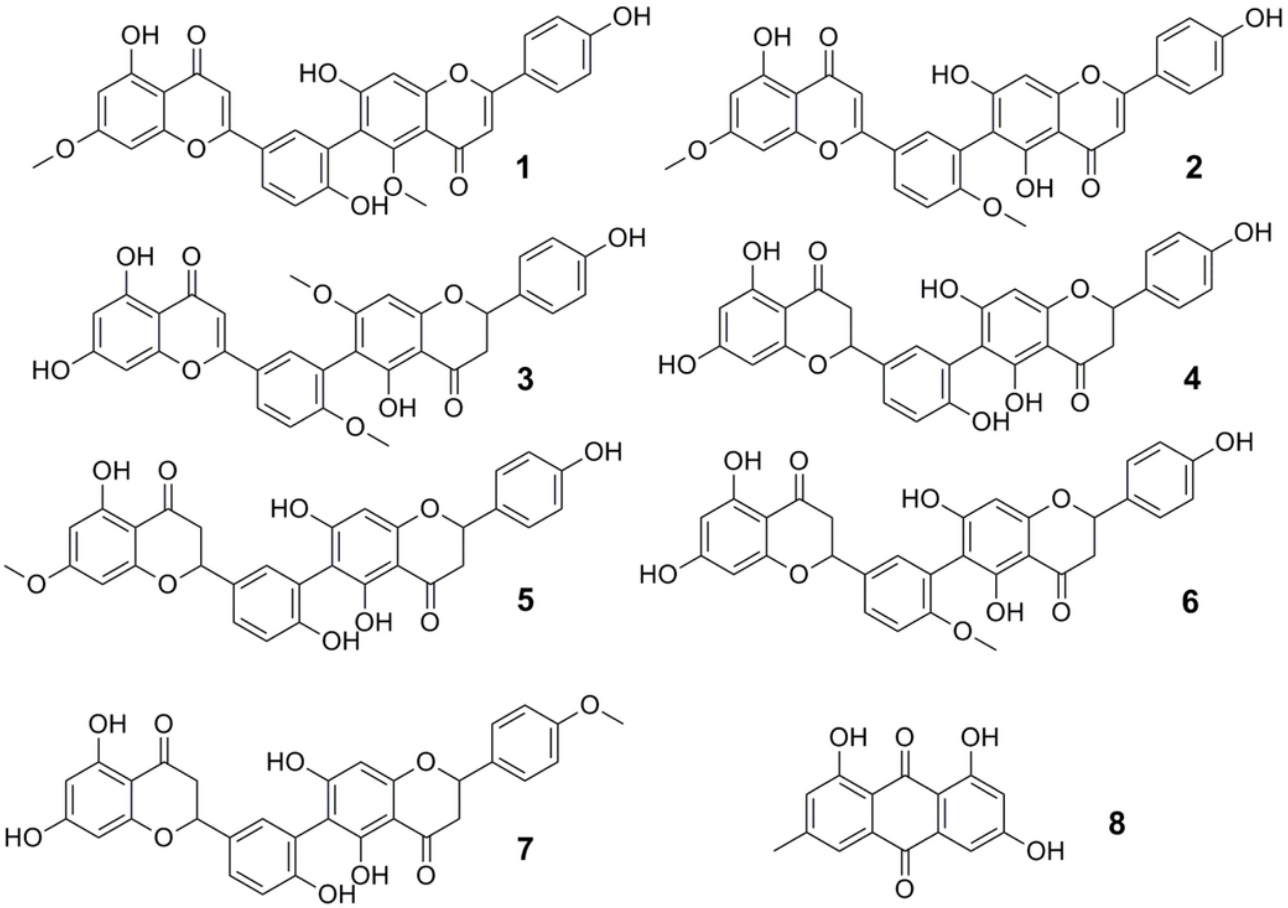

Figure 1

The chemical structure of compounds 1-8. Compounds **1**-**7** are identified as robustaflavone 7,5"-dimethyl ether (**1**), robustaflavone 7,4'-dimethyl ether (**2**), 2",3"-dihydrorobustaflavone 4',7"-dimethyl ether (**3**), 2,3,2",3"-tetrahydrorobustaflavone (**4**), 2,3,2",3"-tetrahydrorobustaflavone 7-methyl ether (**5**), 2,3,2",3"-

tetrahydrorobustaflavone 4'-methyl ether (**6**), 2,3,2",3"-tetrahydrorobustaflavone 4"'-methyl ether (**7**). Compound **8** was identified as anthraquinones, emodin (EG).

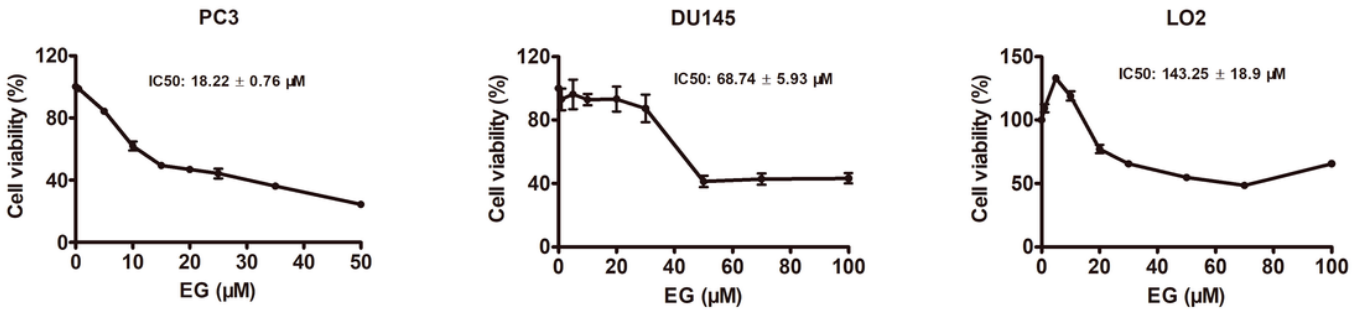

Figure 2

Cell viability assay. PC3, DU145, and LO2 cells were treated with increasing doses of EG and cell viability was assessed using an MTT assay. Data were obtained from three independent experiments and plotted on a graph ($p < 0.05$).

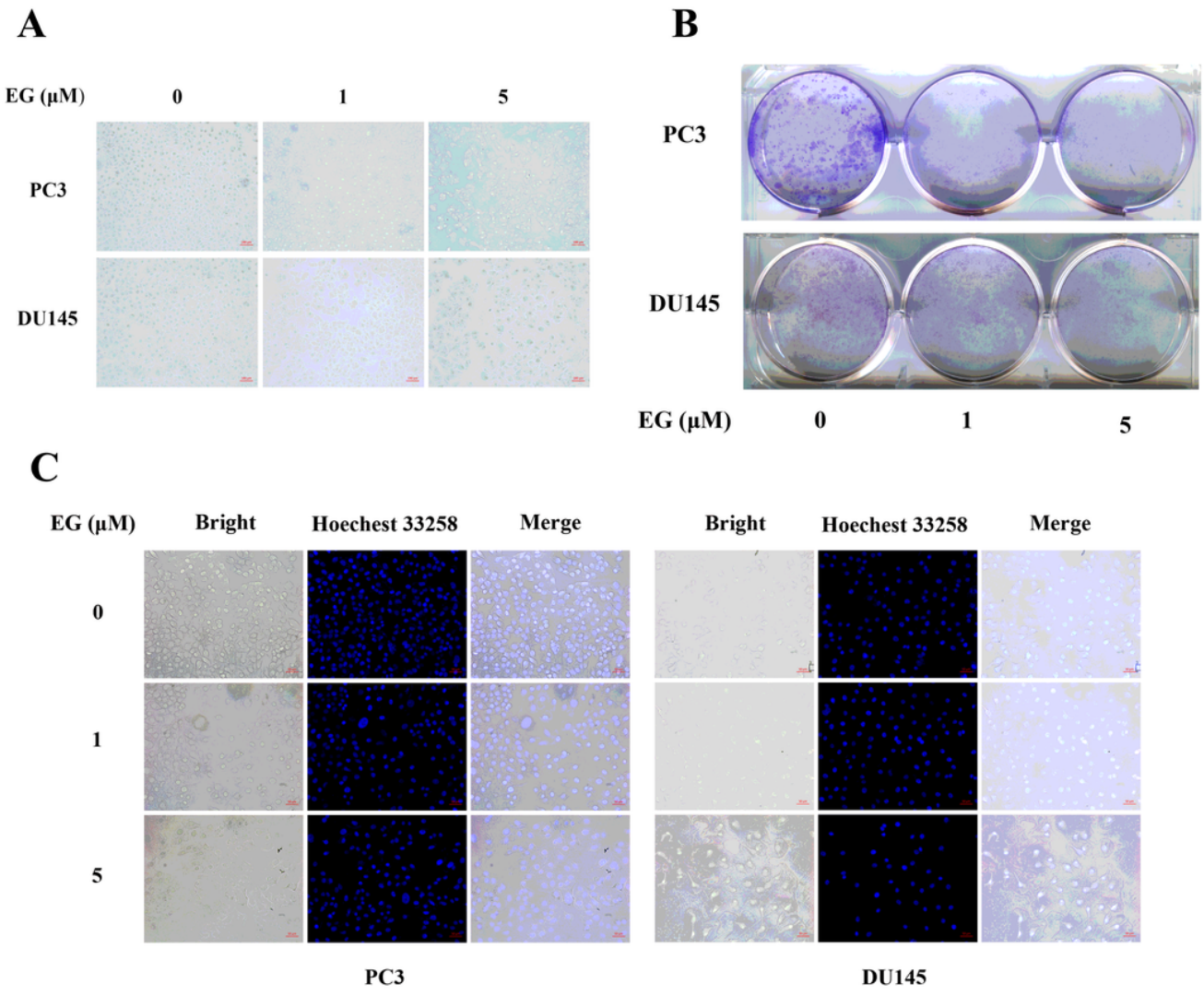

Figure 3

Cell Morphologies analysis. (A) Morphologies of DU145 and PC3 cells were assessed using an inverted microscope after the cells were treated with EG (1 and 5 μM) for 48 h. (B) Colony formation assay was performed after EG-treated DU145 and PC3 cells were incubated for 10-14 days. The colonies were fixed in methanol for 15 min and stained with 0.05% crystal violet and the plates were photographed with a scanner. (C) Fluorescence images of DU145 and PC3 cells after treatment with EG by Hoechest 33258 were photographed under a fluorescence microscope with an excitation wavelength of 330-380nm.

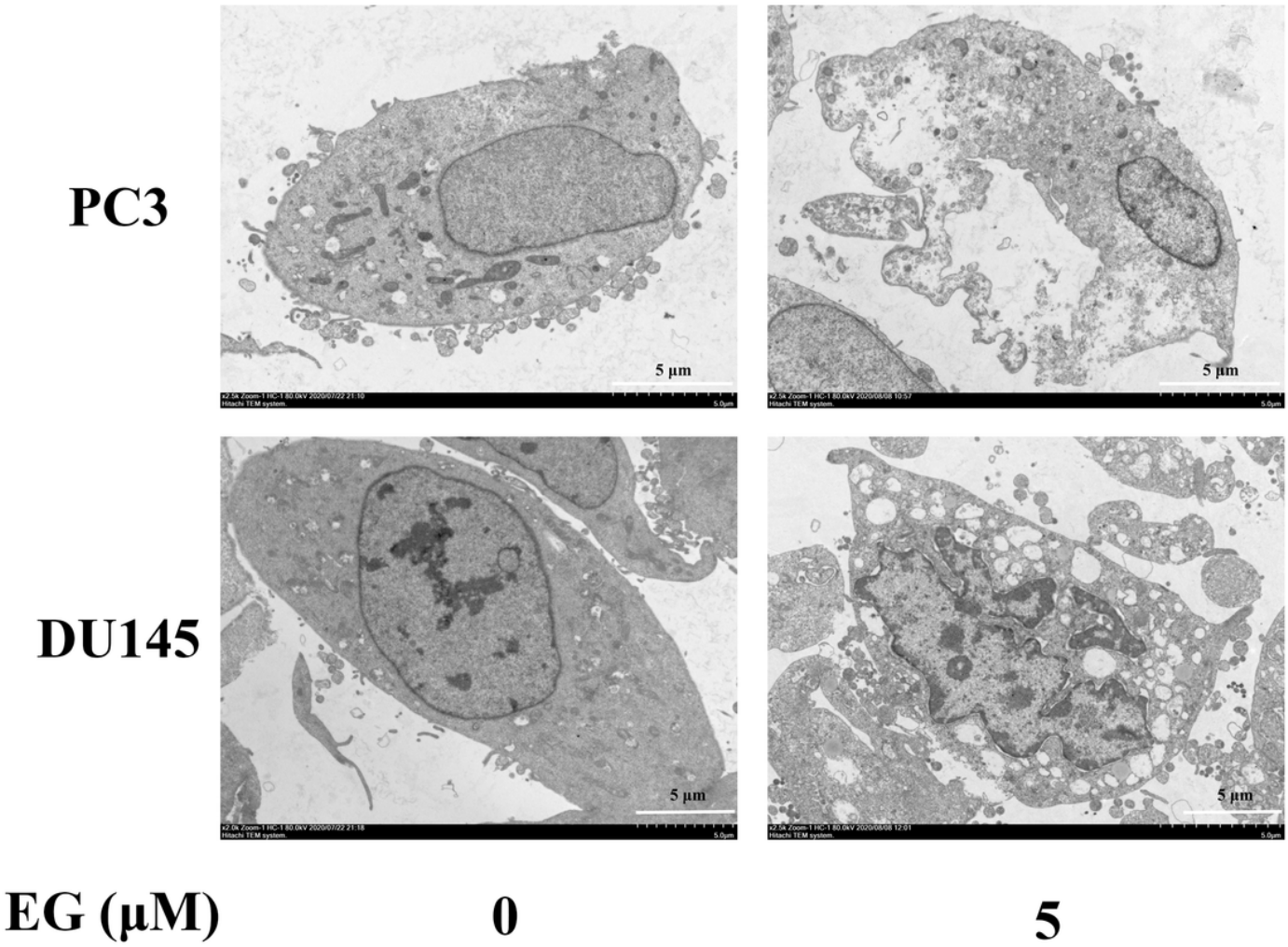

Figure 4

TEM observation. Cells were treated with DMSO and EG and prepared for TEM imaging as described before. The cells were embedded in spur resin and thin sections (50 to 60 nm) were cut, stained with saturated solutions of uranyl acetate combined with lead citrate and observed using TEM HT7700.

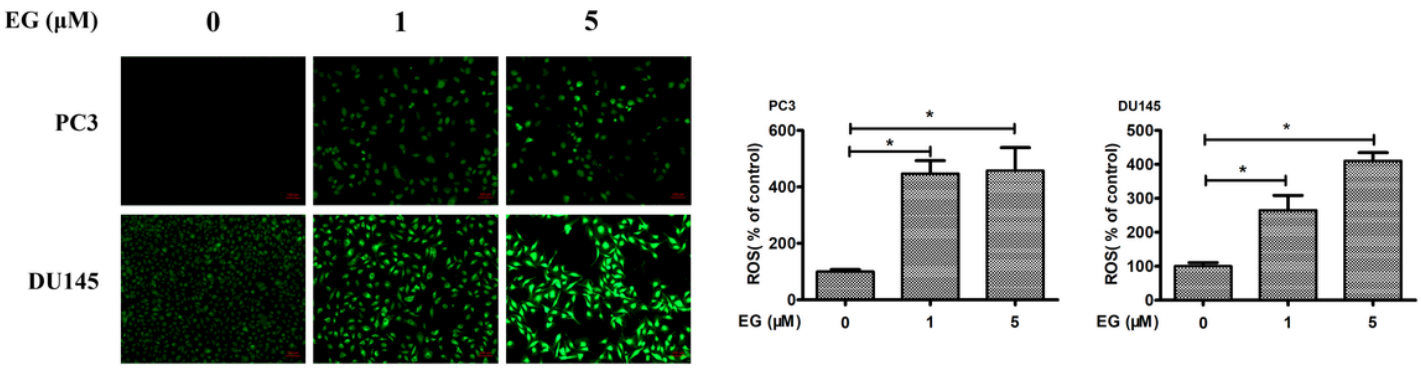

Figure 5

Detection of ROS. Fluorescence images of DU145 and PC3 cells were observed under fluorescence microscopy after cells were treated with EG and subjected to a cellular ROS assay kit. ROS content (%) was measured and plotted on a graph ($p < 0.05$).

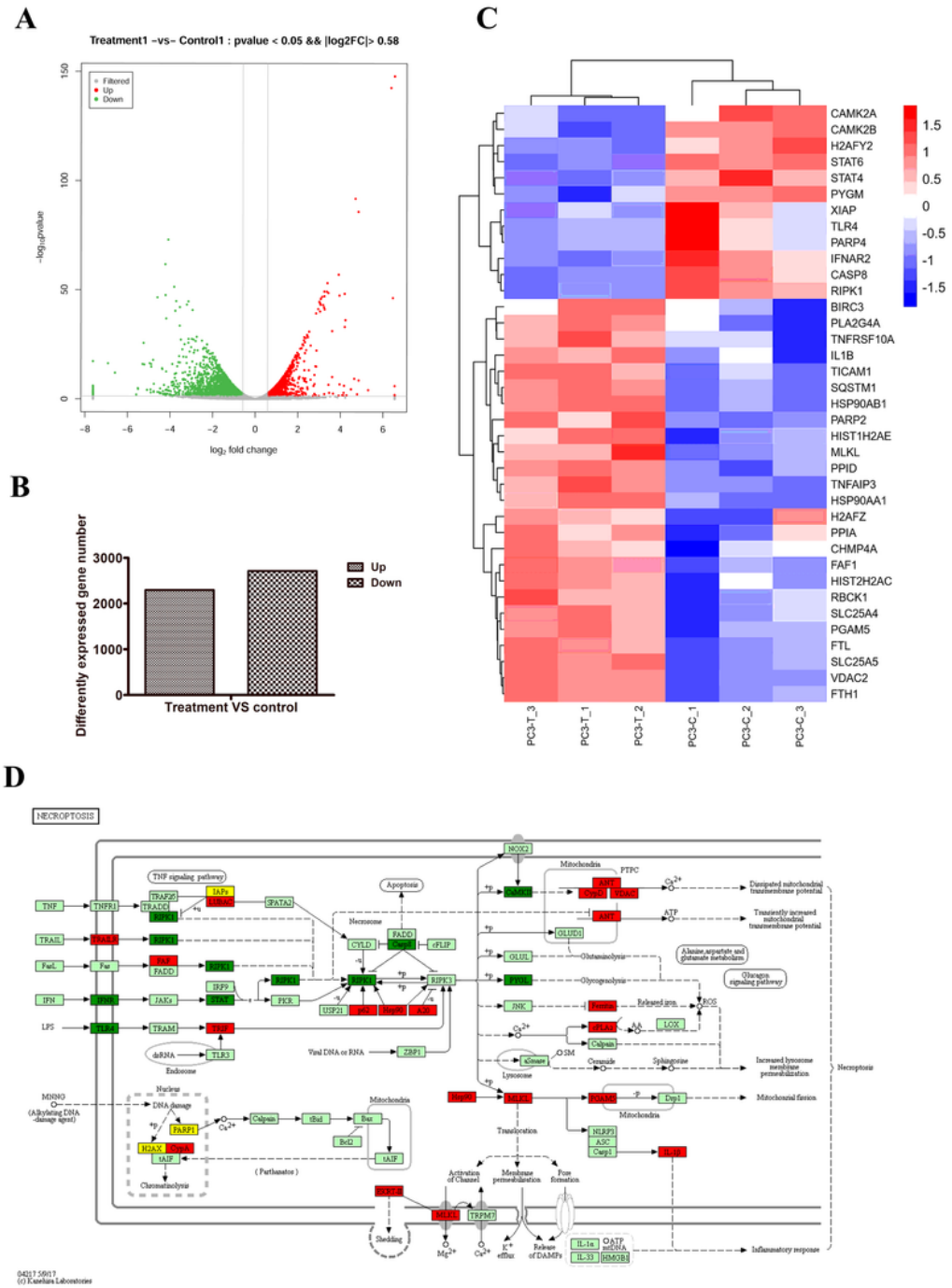

Figure 6

Differentially expressed genes among different groups of PC3 cells from RNA sequencing. Total RNA was extracted using the mirVanaTM miRNA isolation Kit. cDNA libraries were constructed and sequenced on the Illumina sequencing platform. 125bp/150bp paired-end reads were generated. (A) Differentially expressed genes (DEGs) were identified using the DESeq R package functions estimate SizeFactors and nbinomTest. P-value < 0.05 and fold-change > 2 or < 0.5 were set as the threshold for significantly

differential expression and Volcano plot of DEGs was generated. (B) Summary of DEGs numbers was plotted on a bar diagram. (C) Heatmap of DE-mRNAs in PC3 cells between EG treatment group and control group was generated with red and blue color representing down-expression and up-expression, respectively. (D) Functions of differentially expressed genes with enriched KEGG pathway in the necroptosis cell death pathway. Green, red and yellow represent down regulation, up regulation and both up and down regulation, respectively.

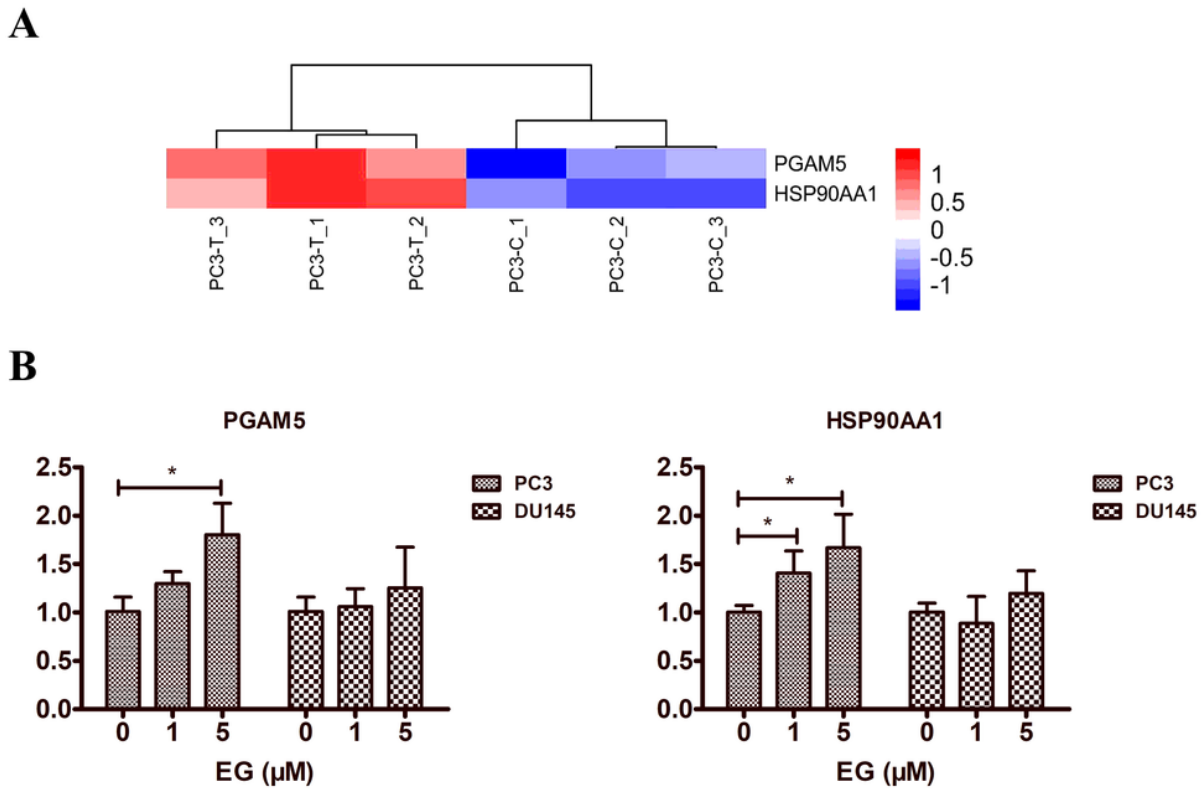

Figure 7

Expression of PGAM5 and HSP90AA1 mRNA. (A) The heatmap of DE-mRNAs between the EG group and the control group. Blue represents the upregulated RNA levels. (B) RT-QPCR results show enhanced PGAM5 and HSP90AA1 mRNA levels in DU145 and PC3 cells in response to EG.

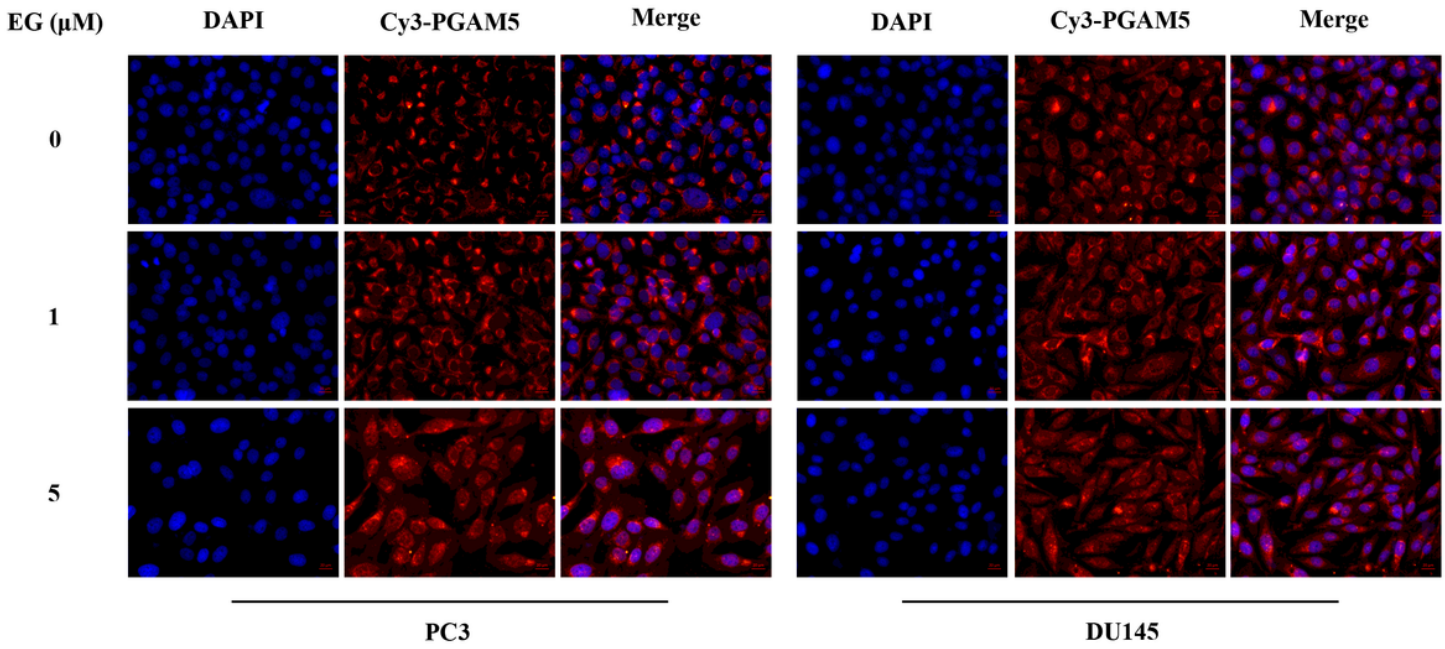

Figure 8

Immunofluorescence assay of PGAM5 protein. DU145 and PC3 cells were treated with different concentrations of EG and immunostained with a PGAM5 antibody. Later, cells were incubated with Cy3–conjugated secondary antibody followed by staining with DAPI and imaging with a fluorescence microscope.

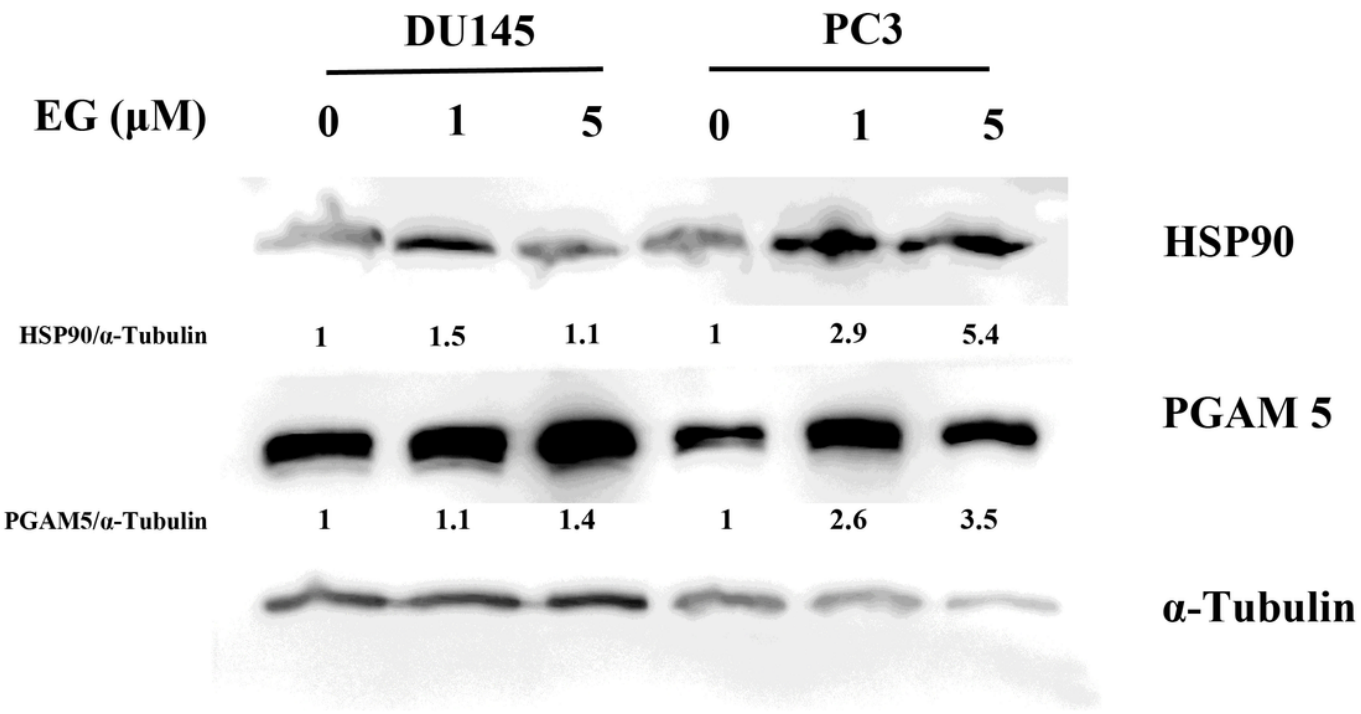

Figure 9

Proteins expressions of HSP90 and PGAM5. DU145 and PC3 cells were treated with different concentrations of EG for 48 h. Total protein was isolated and subjected to Western blotting. a-tubulin was used as control. The protein expression was detected by using an ECL Prime Western blotting Kit.

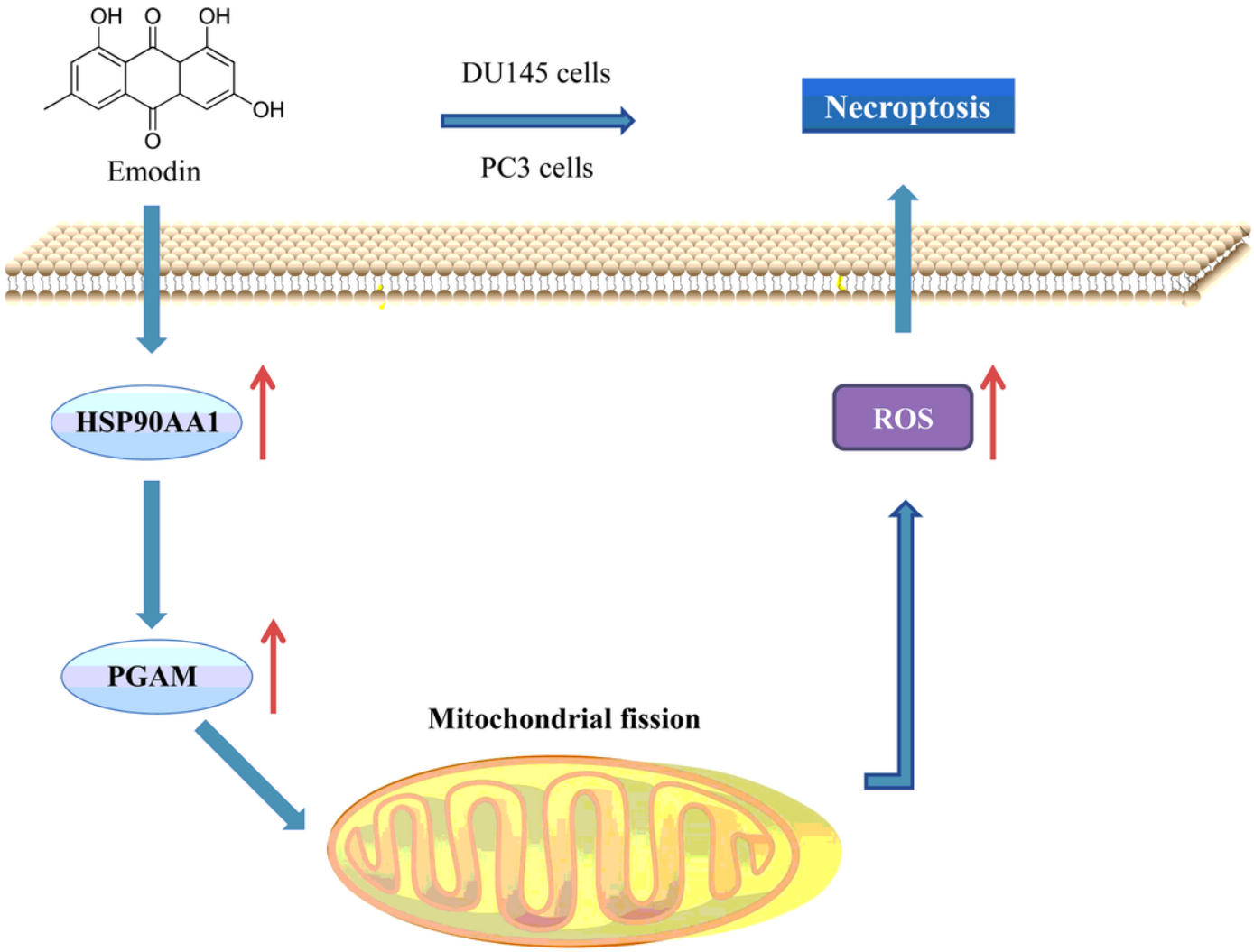

Figure 10

The sketch map of the underlying molecular mechanisms associated with the anticancer effect of EG in PC3 and DU145 cells.